Optics Letters

Ultrasensitive vector bending sensor based on multicore optical fiber

Joel Villatoro,[1,2,*] Amy Van Newkirk,[3] Enrique Antonio-Lopez,[3] Joseba Zubia,[1] Axel Schülzgen,[3] and Rodrigo Amezcua-Correa[3]

[1]Department of Communications Engineering, Escuela Técnica Superior de Ingeniería (ETSI) de Bilbao, University of the Basque Country (UPV/EHU), Alda. Urquijo s/n, E-48013 Bilbao, Spain
[2]IKERBASQUE—Basque Foundation for Science, E-48011 Bilbao, Spain
[3]CREOL, The College of Optics & Photonics, University of Central Florida, P.O. Box 162700, Orlando, Florida 32816-2700, USA
*Corresponding author: agustinjoel.villatoro@ehu.eus

Received 10 November 2015; revised 15 January 2016; accepted 17 January 2016; posted 19 January 2016 (Doc. ID 253666); published 11 February 2016

In this Letter, we demonstrate a compellingly simple directional bending sensor based on multicore optical fibers (MCF). The device operates in reflection mode and consists of a short segment of a three-core MCF that is fusion spliced at the distal end of a standard single mode optical fiber. The asymmetry of our MCF along with the high sensitivity of the supermodes of the MCF make the small bending on the MCF induce drastic changes in the supermodes, their excitation, and, consequently, on the reflected spectrum. Our MCF bending sensor was found to be highly sensitive (4094 pm/deg) to small bending angles. Moreover, it is capable of distinguishing multiple bending orientations.

OCIS codes: (060.2370) Fiber optics sensors; (060.4005) Microstructured fibers; (120.3180) Interferometry; (060.2280) Fiber design and fabrication; (280.4788) Optical sensing and sensors.

http://dx.doi.org/10.1364/OL.41.000832

The continuous monitoring of the verticality (or horizontality) of buildings, towers, bridge piles, and many other infrastructures is important to assess their structural health. For such applications bending or inclination sensors that are highly sensitive and that can resolve small bending angles are desirable. In addition, bending sensors must be compact, simple, accurate, reliable, and, ideally, they must have the capacity to distinguish the bending or inclination orientation. The optical fiber sensor community has long been striving to achieve bending sensors with such features. However, we believe that no such fiber optic bending sensor currently exists that delivers all or most of the aforementioned requirements.

Bending (tilt or inclination) sensors based on fiber Bragg gratings (FBGs) have been demonstrated in different configurations, see for example [1–5]. In general, FBG-based bend sensors exhibit low sensitivity for small angles and typically require additional reference sensors. Directional bending sensors based on long-period gratings (LPGs) [6–12] are highly sensitive, but in most cases their sensitivity to the medium that surrounds the LPG is an issue as it can compromise the sensor performance. Some interferometric bending sensors [13–16] that have been proposed until now are highly sensitive, but they tend to be more complex. Other bending sensors based a conventional fibers codify the bending angle on intensity measurements [17–19]. The disadvantage in this case is the need of compensation mechanisms and the impossibility to distinguish the bending orientation.

Specialty optical fibers such as photonic crystal fibers (PCF) and multicore optical fibers (MCF) offer new possibilities to develop bending sensors [20–29]. The disadvantages of the PCF bending sensors include low reproducibility and high insertion losses [20–24]. Bending sensors based on MCFs with isolated cores [20,25–27] require complex fabrication setups or interrogation systems, while those based on symmetric coupled-core MCFs cannot distinguish the bending orientation [28]. Sensors based on asymmetric MCFs are direction sensitive, but their fabrication may entail a multistep process [29].

In this Letter, we report on a simple interferometric bending sensor based on a MCF consisting of three strongly coupled cores, see Fig. 1. One of the cores is located at the center of the MCF which simplifies the splicing with a conventional single mode optical fiber (SMF).

To fabricate our device, a short segment of the MCF was fusion spliced at the distal end of a standard SMF. After the splicing, the MCF was cleaved so that its end facet acted as a low-reflectivity mirror. The bending sensor reported here has important features which include compactness, ultra high bending angle sensitivity (theoretically up to 6000 pm/deg), operation in a small angle region (±1°), and the capability to distinguish multiple bending orientations. Therefore, we believe that our device overcomes the main limitations of the majority of fiber optic bending sensors reported until now.

The MCF used in our experiments was fabricated using the well-established stack and draw method. The diameter of the MCF cores is 9 μm, the separation between the cores (pitch) is 11 μm, and the MCF diameter is 120 μm. The MCF was

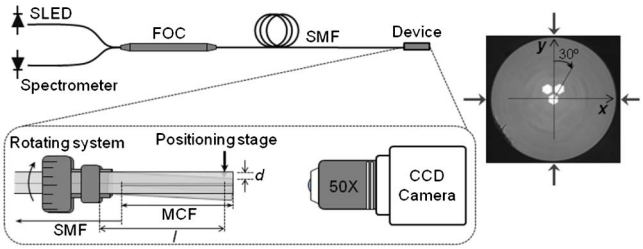

Fig. 1. Sketch of a multicore optical fiber (MCF) interferometer used as a bending sensor. Its interrogation comprises a superluminescent emitting diode (SLED), a fiber optic circulator (FOC), and a spectrometer. The micrograph shows the cross section of the MCF used in the experiments. l and d are, respectively, the distance from the fixing point to the point where the MCF is bent and the displacement of the stage. The arrows in the image indicate the four points where the MCF was bent.

fabricated from Ge-doped silica, the difference in refractive indices between core and cladding (Δn) was 7×10^{-3} and each core had a numerical aperture (NA) of 0.14. Our MCF supports three polarization degenerate supermodes, see Fig. 2. The simulations shown in the figure were calculated for 1550 nm with the finite difference method using commercial waveguide software (FimmWave by Photon Design).

It is important to point out that the NA of our MCF matches that of a standard SMF (which is also 0.14). This, combined with the similar dimensions of our MCF and the SMF, makes the splicing simple and reproducible. To splice our MCF and the SMF. we used the default program for splicing single mode fibers set up in a commercially available splicing machine (Fujikura FSM 100$P+$) with the only difference being that we used the cladding alignment method. The splice loss in our case was ~0.1 dB.

The working mechanism of our interferometer is simple. The fundamental mode of the SMF excites supermodes in the MCF [29] which propagate along the MCF and are reflected back from the cleaved MCF end into the SMF. The interference between the MCF supermodes gives rise to a periodic coupling of the power back into the SMF core. The modes excited in the MCF have different propagation constants which depend on the wavelength of the optical source. Thus, the MCF acts in a similar manner to a directional coupler [28,29]. Therefore, the reflected spectrum of our interferometer is expected to exhibit periodic maximums and minimums. However, by using a short segment of MCF (16 mm in our case), the spectral period of the interference pattern will be large, as shown in Fig. 3, where only one minimum can be seen at about 1565 nm. The spectra shown in Fig. 3 were obtained by launching light from a low-power superluminescent emitting diode (SLED) (Safibra s.r.o.) centered at 1550 nm to the MCF by means of a fiber optic

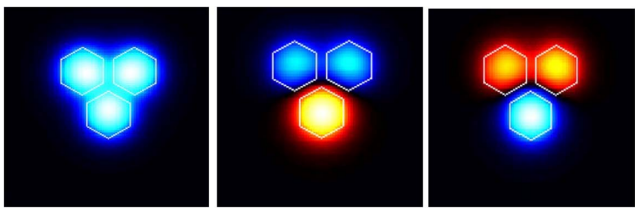

Fig. 2. Simulated mode profiles of the three polarization degenerate supermodes supported by the three-core MCF shown in Fig. 1.

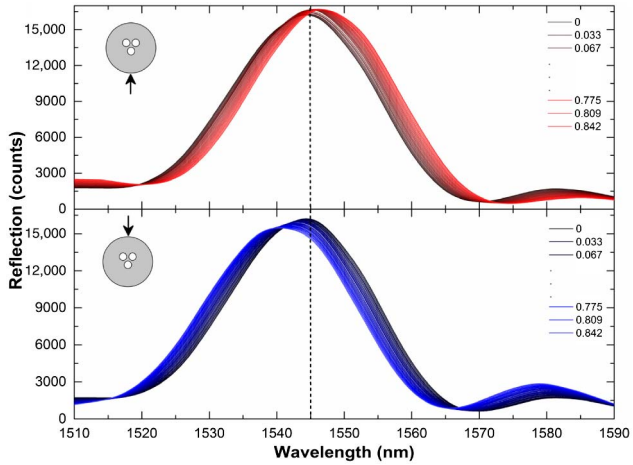

Fig. 3. Interference patterns observed when the MCF was bent in the $+y$ direction (top graph) and the $-y$ direction (bottom graph). All angles are given in degrees. The inset drawings show the points where the MCF was bent. The vertical dotted line shows the position of the spectra when the MCF is straight. The length of MCF was 16 mm in all cases.

circulator. The reflected light was analyzed with a single-channel, miniature spectrometer (I-MON-512 USB from IBSEN Photonics) connected to a personal computer.

To investigate the performance of our interferometer as a bending sensor we placed it in a cantilever-like position, see Fig. 1. To do so, our device was immobilized with an optical fiber rotator (HFR007, Thorlabs). The cleaved end of the MCF was observed with a 50× microscope objective attached to a change-coupled device (CCD) camera (DCU224C, Thorlabs). Before introducing bending to the MCF, the cores of the fiber were oriented in a V-like configuration, i.e., two cores on top of the central core, see Fig. 1. The core orientation was done fast as the MCF could be rotated easily. The reason for such orientation will be explained in the following paragraphs.

Bending to the MCF was introduced with precise micropositioners (3-Axis NanoMax Stage, Thorlabs). Our set up allowed us to bend the MCF vertically (in the $+y$ and $-y$ directions) and horizontally (in the $+x$ and $-x$ directions). The bending angle was varied with d (the distance traveled by the translation stage) as l (the distance from the point when the MCF is immobilized to the point where it is bent) was fixed, see Fig. 1.

The results of our experiments are shown in Fig. 3. Note that when the MCF was bent to the $+y$ direction, the reflection spectra shift to longer wavelengths (red shift) and when the device was bent to the $-y$ direction the interference patterns shift to shorter wavelengths (blue shift). The shifts observed as a function of the bending angle for both directions are shown in Fig. 4. Regardless, the direction of the bending in a linear behavior was observed. The bending sensitivities were found to be $+3890$ pm/deg when the bending was in the $+y$ direction and -4094 pm/deg when the bending was in the $-y$ direction.

The curvature sensitivities of our MCF are ~ -1.99 nm/m^{-1} and $\sim +1.90$ nm/m^{-1} for the $-y$ and $+y$ direction, respectively. Such sensitivities were calculated by assuming that the radius of curvature (R) of our MCF can be expressed as [15]: $R \approx l^2/(2d)$ which is valid when $d \ll l$. The above sensitivities are higher than those of the ultrasensitive LPG-based bending sensor reported in [26].

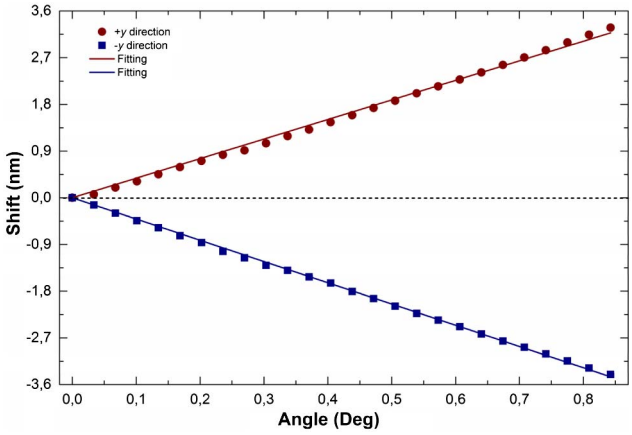

Fig. 4. Shift of the interference pattern as a function of the bending angle when the bending was in the $+y$ direction (dots) and the $-y$ direction (squares). The solid lines are linear fittings to the experimental data.

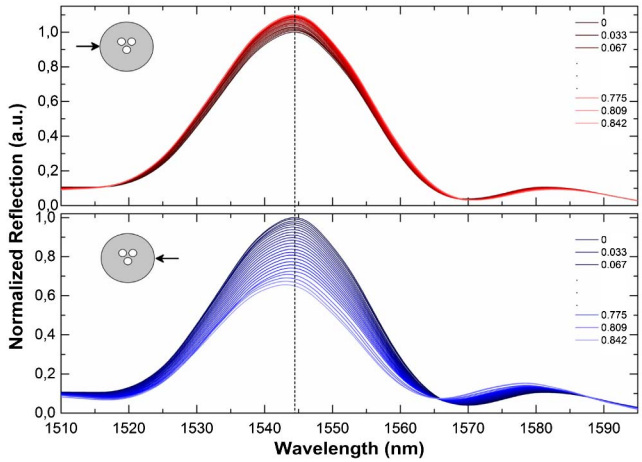

Fig. 5. Interference patterns observed when the interferometer was bent in the $+x$ direction (top graph) and $-x$ direction (bottom graph) according to the coordinate system shown in Fig. 1. The length of the MCF was 16 mm in all cases. The orientation of the MCF cores is illustrated by the inset drawings. The vertical line shows the position of the maximum when the MCF was straight.

The origin of the red or blue shift of the interference patterns can be explained by means of the conformal mapping technique [30,31]. This technique replaces the curved waveguide by an equivalent straight one with an index profile that depends on R. Thus, the refractive index distribution of the mth MCF core can be expressed as [32,33]: $n' \approx n_m(1 + y/R)$ when the fiber is bent in the $+y$ direction. n_m is the index of the mth core when it is straight. The geometrical center of the MCF is considered at the point $y = 0$. Therefore, if the MCF is bent in the $+y$ direction, see Fig. 1, the refractive index of the three cores will increase in the $+y$ direction in a gradual manner. However, the changes will be more prominent in the two cores on top of the central one as they are further away from the geometrical center of the MCF. When the bending is in the $-y$ direction, the central core will experience larger index changes than the other two cores.

The index changes experienced by the cores of the MCF modify the profile of the supermodes, their propagation constants, and the numerical aperture of the cores. As a consequence, the coupling between the supermodes is altered, given rise to a shift of the reflected interference pattern. The interference pattern shifts to longer wavelengths when the index of the supermodes increases, which happens when the bending is in the $+y$ direction.

The MCF was also bent in the $+x$ and $-x$ directions (according to the coordinate system shown in the micrograph of Fig. 1). The results of the experiments are shown in Fig. 5. In these cases the shift of the interference patterns is minimal and the changes in intensity are prominent. The more dramatic changes occur when the MCF is bent in the $-x$ direction. Figure 6 shows the changes in the absolute maximum (1 is considered when the MCF is not bent) of the reflected pattern as a function of the bending angle. Again, an approximately linear behavior was observed. The lack of wavelength shift in these directions can be explained by the fact that the MCF is symmetric in the x-axis, so the interfering supermodes change by the same amount, leading to no change in the supermode interference spectral pattern.

From the above results, it is not difficult to conclude that the bending of our device in any other random direction will cause a mixture of amplitude and shifting of the interference pattern. Thus, by combining the intensity interrogation with the spectral interrogation, one could, in principle, know any of the bending directions. Moreover, by optimizing the structure of the MCF (core size and core-to-core separation) the performance of the bending sensor proposed here can be further enhanced.

The bending sensitivities of our device were verified through simulation by using commercial waveguide software, FimmWave by Photon Design, which uses the finite difference method to calculate the modes of an optical fiber. The SMF and MCF were simulated and the fiber chain was created. The device spectra were then calculated as the MCF was bent in the four directions mentioned above. Figure 7 summarizes our results. Our simulation predicts a blue shift when the MCF is bent in the $-y$ direction and a red shift when the fiber is bent in the $+y$ direction. The theoretical sensitivities for the $+y$ and $-y$ directions are 6000 pm/deg and −6000 pm/deg, respectively.

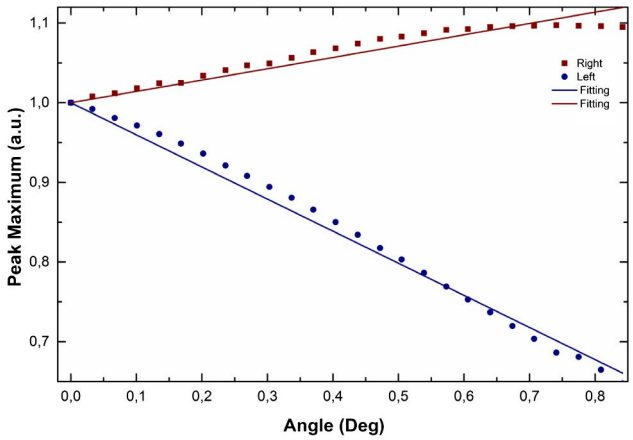

Fig. 6. Relative changes of the reflected spectra observed when the interferometer was bent in the $+x$ direction (squares) and $-x$ direction (solid dots) according to the micrograph shown in Fig. 1. The length of MCF was 16 mm in all cases.

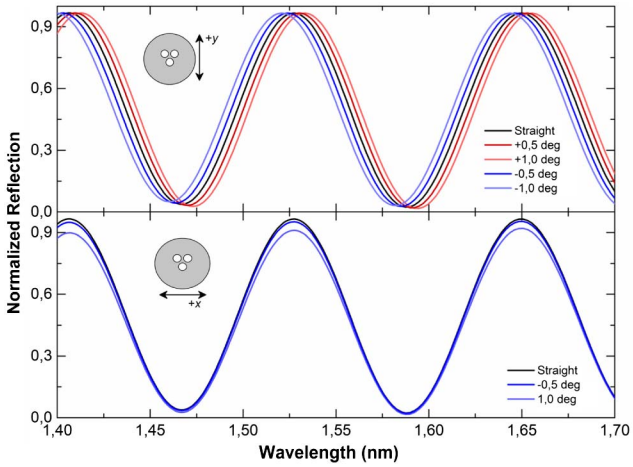

Fig. 7. Theoretical interference patterns of a three-core MCF when it is straight and when it is bent 0.5 and 1 deg in the $+y$ and $-y$ direction (top graph) or in the $-x$ direction (bottom graph). The length of the MCF was assumed to be 16 mm in all cases.

It can be noted that the experimental results agree well with the numerical ones, but with lower sensitivity and less symmetry between the measurements. As for the x direction, both the positive and negative direction showed no wavelength shift, but an overall decrease of about 6% in power when the MCF was bent by 1 deg, see Fig. 7. The differences between theoretical and experimental results (for bending in the x direction) can be explained by the difference between the ideal MCF used in the simulation and the real MCF used in the experiments. In addition, in the simulations the role of the SMF-MCF junction was not taken into account which may be altered during the bending experiments. Another factor that may affect the experimental results is the fact that the MCF was not perfectly vertically aligned during the experiments.

The results shown in Figs. 3–7 suggest that by monitoring the relative changes in the reflected power or the shift of the interference pattern, one can distinguish if the fiber is bent to the north ($+y$ direction), south ($-y$ direction), east, or west (x direction), i.e., to the four cardinal points.

The sensitivity of our device to environmental disturbances (e.g., temperature) or the influence of fluctuations of the optical source can be easily compensated. Temperature can cause a shift of the interference pattern, but it does not change the amplitude of the same. On the other hand, fluctuations of the optical source do not cause a shift of the interference pattern.

In a practical situation the MCF bending sensor proposed here must be properly packaged. Our MCF is not sensitive to the surrounding environment, thus, packaging materials may not affect the device performance. The orientation of the cores of the MCF is not an issue, as it can be carried out with the same technology used in modern optical fiber splicing machines.

In conclusion, we have reported on a bending sensor based on a MCF with an asymmetric core distribution. The cores of the MCF were aligned in a V-like configuration. The main features of the sensor reported here are: (i) compactness, a few millimeters of MCF are needed to fabricate the sensor, (ii) ultra high bending angle sensitivity (up to -4094 pm/deg), (iii) capability to distinguish multiple bending directions, and (iv) simple fabrication (a single splice is required) and interrogation of the sensor. Our sensor has the potential to monitor other parameters that can be converted to bending angles. Thus, we believe that it can be used in applications where ultra high and bend-direction sensitivity are required.

Funding. FEDER Funds; University of the Basque Country (UFI11/16US13/09, EUSKAMPUS); Ikerbasque, Basque Foundation for Science; Ministerio de Economía y Competitividad (MINECO) (TEC2015-63826-C3-1); Eusko Jaurlaritza (IT664-13, ELKARTEK).

REFERENCES

1. X. Dong, Y. Liu, Z. Liu, and X. Dong, Opt. Commun **192**, 213 (2001).
2. L.-Y. Shao and J. Albert, Opt. Lett. **35**, 1034 (2010).
3. X. Chen, C. Zhang, D. J. Webb, K. Kalli, and G.-D. Peng, IEEE Photon. Technol. Lett. **22**, 850 (2010).
4. A. Rauf, J. Zhao, B. Jiang, Y. Jiang, and W. Jiang, Opt. Lett. **38**, 214 (2013).
5. W. Cui, J. Si, T. Chen, and X. Hou, Opt. Express **23**, 11031 (2015).
6. H. J. Patrick, C. C. Chang, and S. T. Vohra, Electron. Lett. **34**, 1773 (1998).
7. C. C. Ye, S. W. James, and R. P. Tatam, Opt. Lett. **25**, 1007 (2000).
8. T. Allsop, A. Gillooly, V. Mezentsev, T. Earthgrowl-Gould, R. Neal, D. J. Webb, and I. Bennion, IEEE Trans. Instrum. Meas. **53**, 130 (2004).
9. Y. P. Wang and Y. J. Rao, IEEE Sens. J. **5**, 839 (2005).
10. L. Jin, W. Jin, and J. Ju, J. Lightwave Technol. **27**, 4884 (2009).
11. L.-Y. Shao, A. Laronche, M. Smietana, P. Mikulic, W. J. Bock, and J. Albert, Opt. Commun. **283**, 2690 (2010).
12. Q. Zhou, W. Zhang, L. Chen, Z. Bai, L. Zhang, L. Wang, B. Wang, and T. Yan, IEEE Photon. Technol. Lett. **27**, 713 (2015).
13. D. Inaudi and B. Glisic, Proc. SPIE **4694**, 36 (2002).
14. L. Yuan, J. Yang, Z. Liu, and J. Sun, Opt. Lett. **31**, 2692 (2006).
15. H. Qu, G. F. Yan, and M. Skorobogatiy, Opt. Lett. **39**, 4835 (2014).
16. L. Zhang, W. Zhang, L. Chen, T. Yan, L. Wang, B. Wang, and Q. Zhou, IEEE Photon. Technol. Lett. **27**, 1240 (2015).
17. K. S. C. Kuang, W. J. Cantwell, and P. J. Scully, Meas. Sci. Technol. **13**, 1523 (2002).
18. A. Khiat, F. Lamarque, C. Prelle, N. Bencheikh, and E. Dupont, Meas. Sci. Technol. **21**, 025306 (2010).
19. Y. G. Lee, H. K. Jang, D. H. Kim, and C. G. Kim, Sens. Actuators A **184**, 46 (2012).
20. B. M. Blanchard, J. G. Burnett, G. R. G. Erry, A. H. Greenaway, P. Harrison, B. Mangan, J. C. Knight, P. St. J. Russell, M. J. Gander, R. McBride, and J. D. C. Jones, Smart Mater. Struct. **9**, 132 (2000).
21. Z. L. Ou, Y. Yu, P. Yan, J. Wang, Q. Huang, X. Chen, C. Du, and H. Wei, Opt. Express **21**, 23812 (2013).
22. H. Gong, H. Song, X. Li, J. Wang, and X. Dong, Sens. Actuators A **195**, 139 (2013).
23. Q. Huang, Y. Yu, X. Li, X. Chen, Y. Zhang, W. Zhou, and C. Du, Opt. Express **23**, 3010 (2015).
24. J. Villatoro, V. P. Minkovich, and J. Zubia, Opt. Lett. **40**, 3113 (2015).
25. M. J. Gander, W. N. Macpherson, R. McBride, J. D. C. Jones, L. Zhang, I. Bennion, P. M. Blanchard, J. G. Burnett, and A. H. Greenaway, Electron. Lett. **36**, 120 (2000).
26. P. Saffari, T. Allsop, A. Adebayo, D. Webb, R. Haynes, and M. M. Roth, Opt. Lett. **39**, 3508 (2014).
27. D. Barrera, I. Gasulla, and S. Sales, J. Lightwave Technol. **33**, 2445 (2015).
28. G. Salceda, A. Van Newkirk, J. Antonio-Lopez, A. Martínez-Rios, A. Schülzgen, and R. Amezcua, Opt. Lett. **40**, 1468 (2015).
29. A. Van Newkirk, J. Antonio-Lopez, A. Velazquez-Benitez, J. Albert, R. Amezcua-Correa, and A. Schülzgen, Opt. Lett. **40**, 5188 (2015).
30. M. Heiblum and J. H. Harris, IEEE J. Quantum Electron. **11**, 75 (1975).
31. K. Nagano, S. Kawakami, and S. Nishida, Appl. Opt. **17**, 2080 (1978).
32. R. T. Schermer, Opt. Express **15**, 15674 (2007).
33. R. T. Schermer and J. H. Cole, IEEE. J. Quantum Electron. **43**, 899 (2007).